Lecture 13

stellar atmospheres

prof. Marcos Diaz

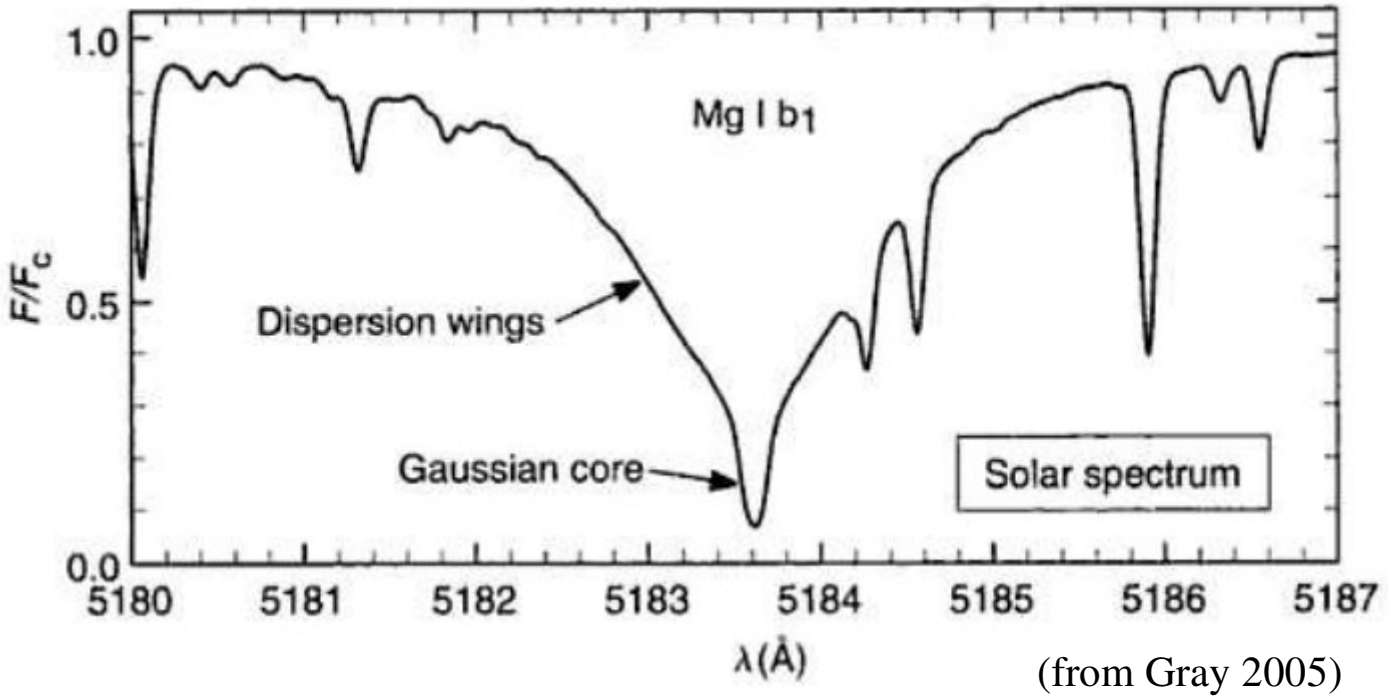

(from Gray 2005)

treasure map:

Gray: 458
Böhm-Vitense: pg 125
Rutten: pg 123

Macroscopic Line Broadening

I. Stellar rotation (cont.)

The rotation profile in reciprocal space

$$\mathscr{F}\left[H(\lambda)*G(\lambda)\right] = \mathscr{F}\left[H(\lambda)\right].\mathscr{F}\left[G(\lambda)\right]$$

(from Gray 2005)

=> broad boxing envelope times the Fourier transform of the rotation kernel (elliptical function).

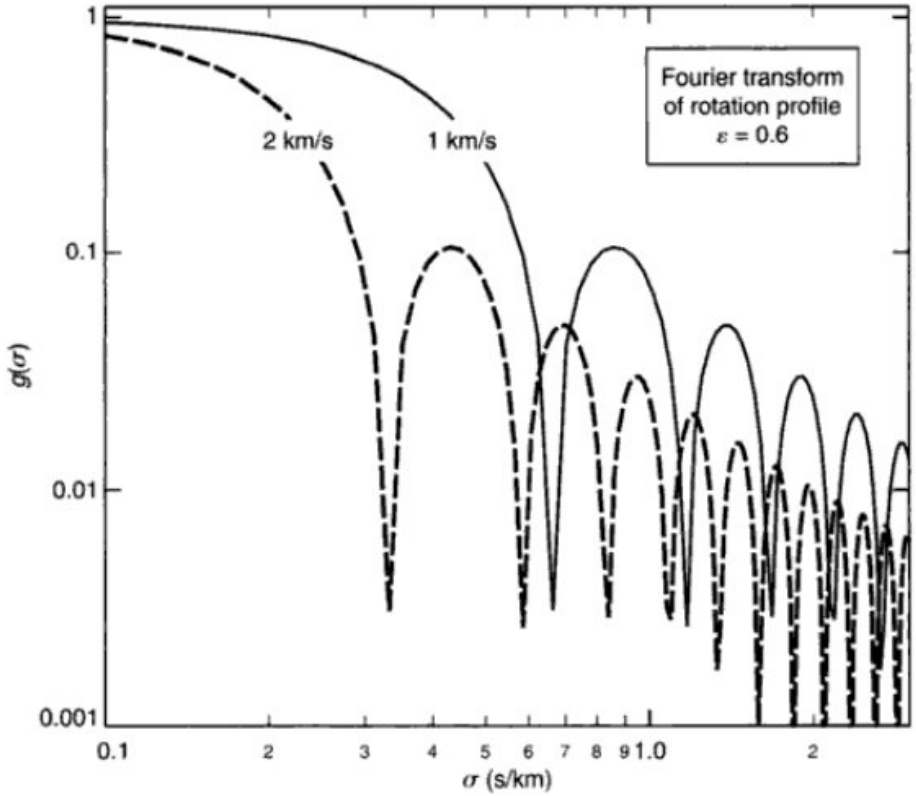

$$\left|\mathscr{F}\left[G(\lambda-\lambda_0)\right]\right| = g(\sigma)$$

with zeros @ $i/\Delta\lambda_L$ $i \in \mathbb{Z}$

$$\Delta\lambda_L = \frac{\lambda}{c} v_{rot} \sin(i)$$

Macroscopic Line Broadening

I. Stellar rotation (cont.)

The rotation profile in reciprocal space

(from Gray 2005)

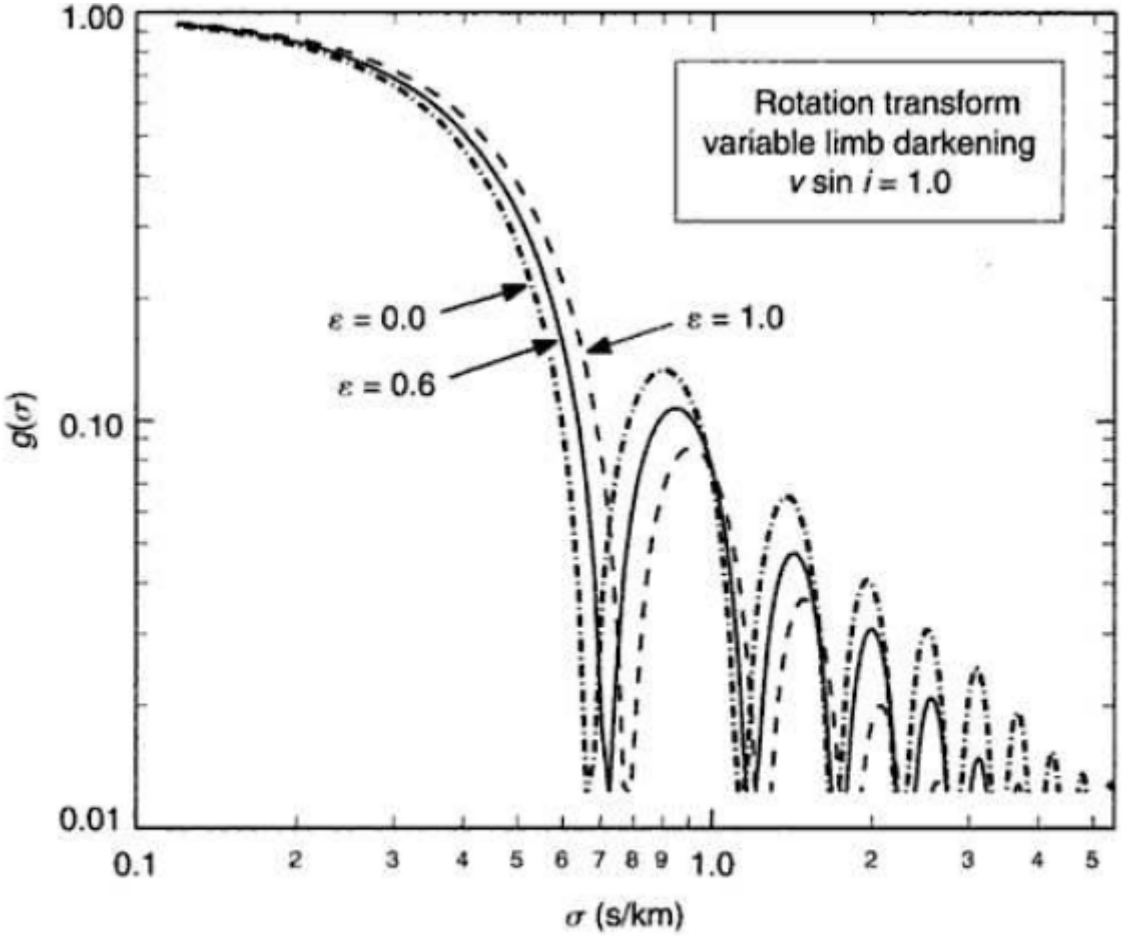

Fig. 18.17. Transforms of the rotation profile depends on the limb darkening coefficient ε. The uniform or undarkened case has $\varepsilon = 0$, while the "fully darkened" extreme has $\varepsilon = 1.0$. When the limb contributes less light, the Doppler shifts at the equatorial limb are weighted less, and the Doppler-shift distribution is narrower, resulting in a wider transform.

Combined multiple line profile analysis

advantage: *Parceval theorem (efficient flux → Ω constraint)*

disadvantage: Mix lines with different broadening contributions

$$D(\lambda) = H(\lambda) * G(\lambda) * I(\lambda)$$

$$\mathcal{F}\left[H(\lambda) * G(\lambda) * I(\lambda)\right] = \mathcal{F}\left[H(\lambda)\right].\mathcal{F}\left[G(\lambda)\right].\mathcal{F}\left[I(\lambda)\right]$$

$$d(\sigma) = g(\sigma).h(\sigma).i(\sigma)$$

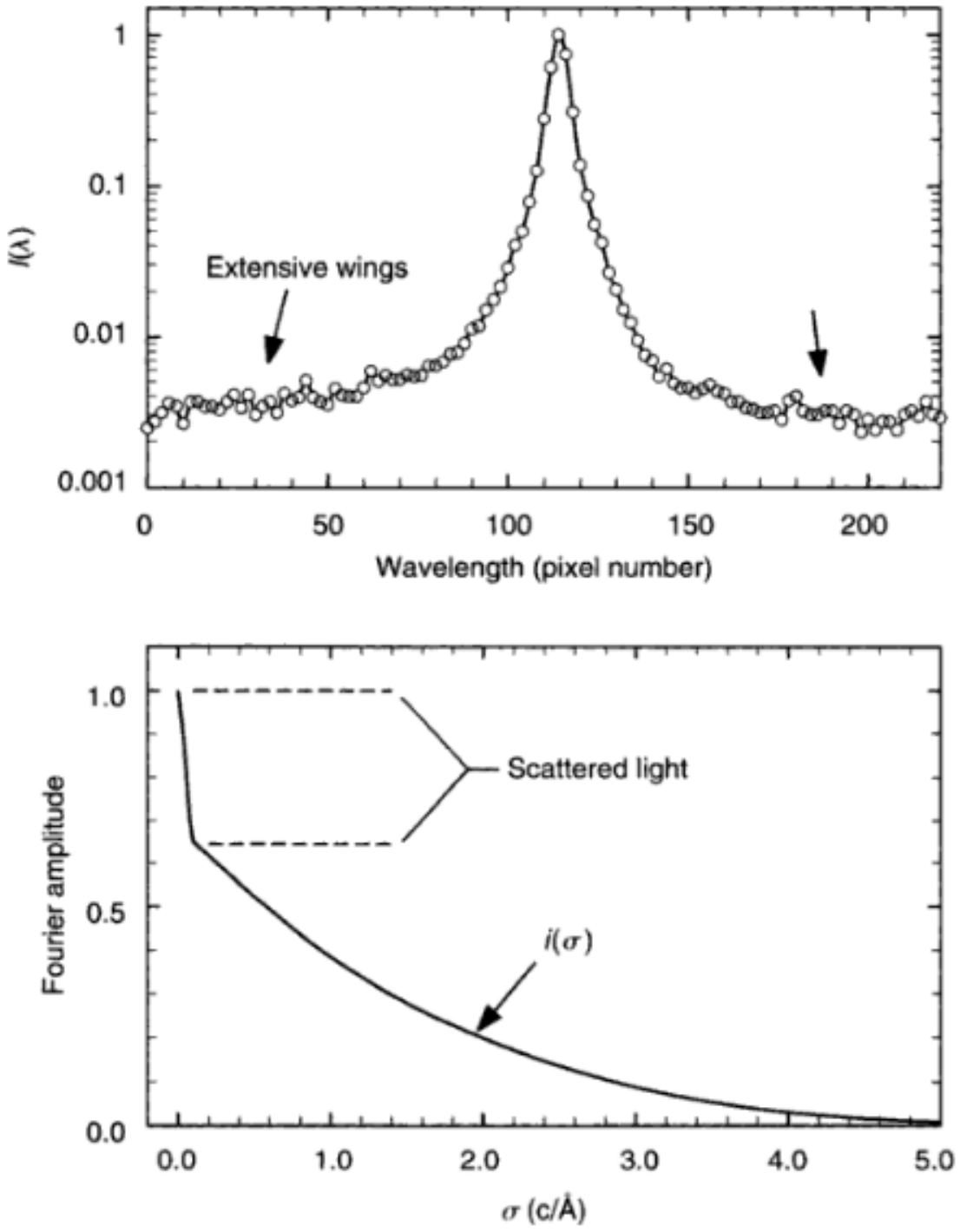

(from Gray 2005)

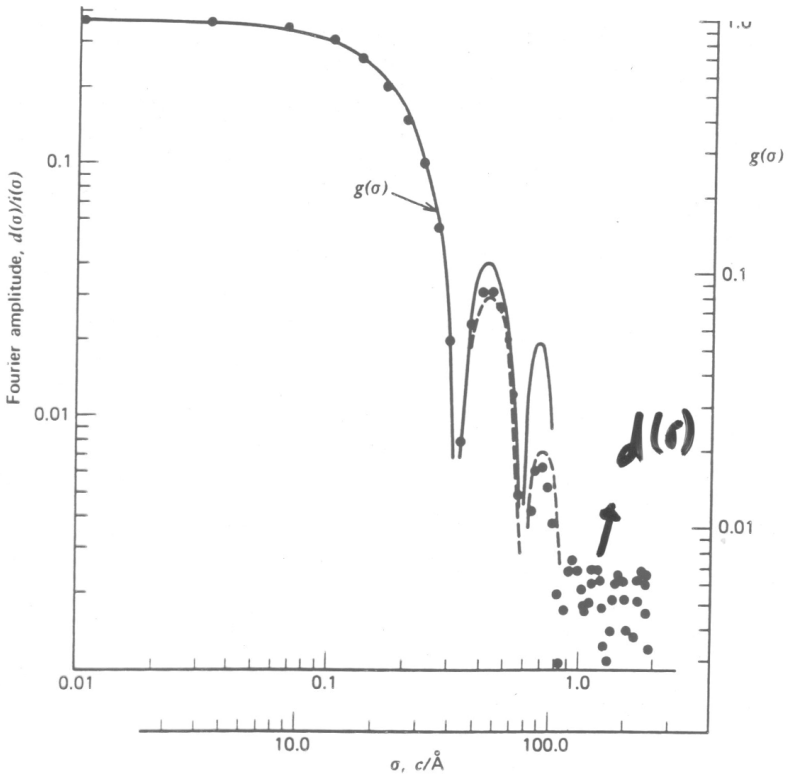

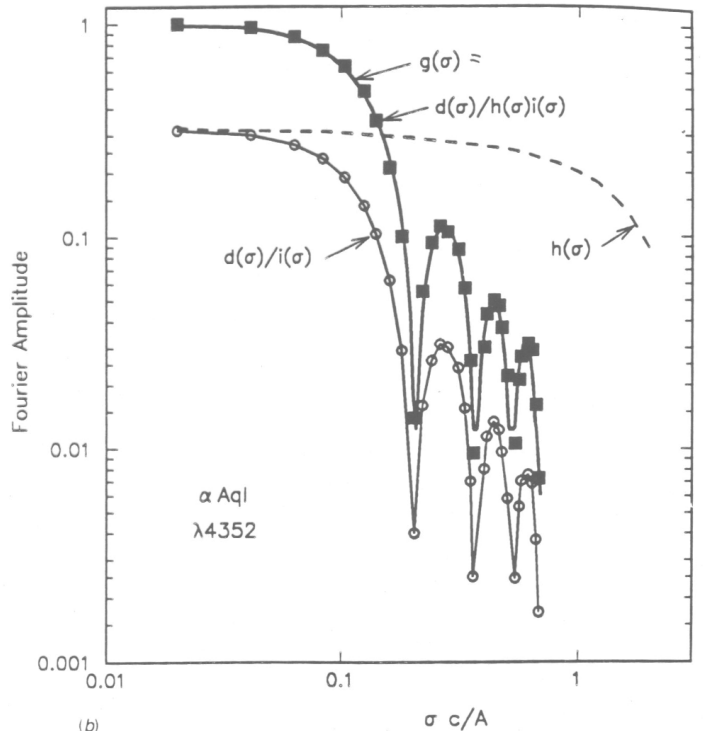

(from Gray 2005)

II. Macroturbulence

A path to asymmetric profile formation

$\Delta l_k > l_\nu$ → local profile shifted by the medium velocity

Similar to rotation kernel convolution
–> with a gaussian distribution of macroturbulent velocities ζ
over the stellar atmosphere.

$$\zeta^2 = \zeta_{tang}^2 + \zeta_{rad}^2 ; \qquad \Delta\lambda = -\frac{\zeta\lambda}{c}$$

$$\Theta(\Delta\lambda) = A_{rad}\Theta_{rad}(\Delta\lambda) + A_{tang}\Theta_{tang}(\Delta\lambda) \qquad \zeta_T = \frac{\zeta_{tang}\lambda}{c}; \qquad \zeta_R = \frac{\zeta_{rad}\lambda}{c}$$

$$= \frac{A_R}{\pi^{1/2}\zeta_R \cos\theta} e^{-(\Delta\lambda/\zeta_R\cos\theta)^2} + \frac{A_T}{\pi^{1/2}\zeta_T \sin\theta} e^{-(\Delta\lambda/\zeta_T\sin\theta)^2}$$

where $cos(\theta) = \mu$

and flux integral over the visible hemisphere:

$$\mathfrak{F}_\nu = 2\pi A_R \int_0^{\pi/2} \Theta_R(\Delta\lambda) * I_\nu \sin\theta \cos\theta \, d\theta$$
$$+ 2\pi A_T \int_0^{\pi/2} \Theta_T(\Delta\lambda) * I_\nu \sin\theta \cos\theta \, d\theta$$

macroturbulent velocities increase with temperature and luminosity class

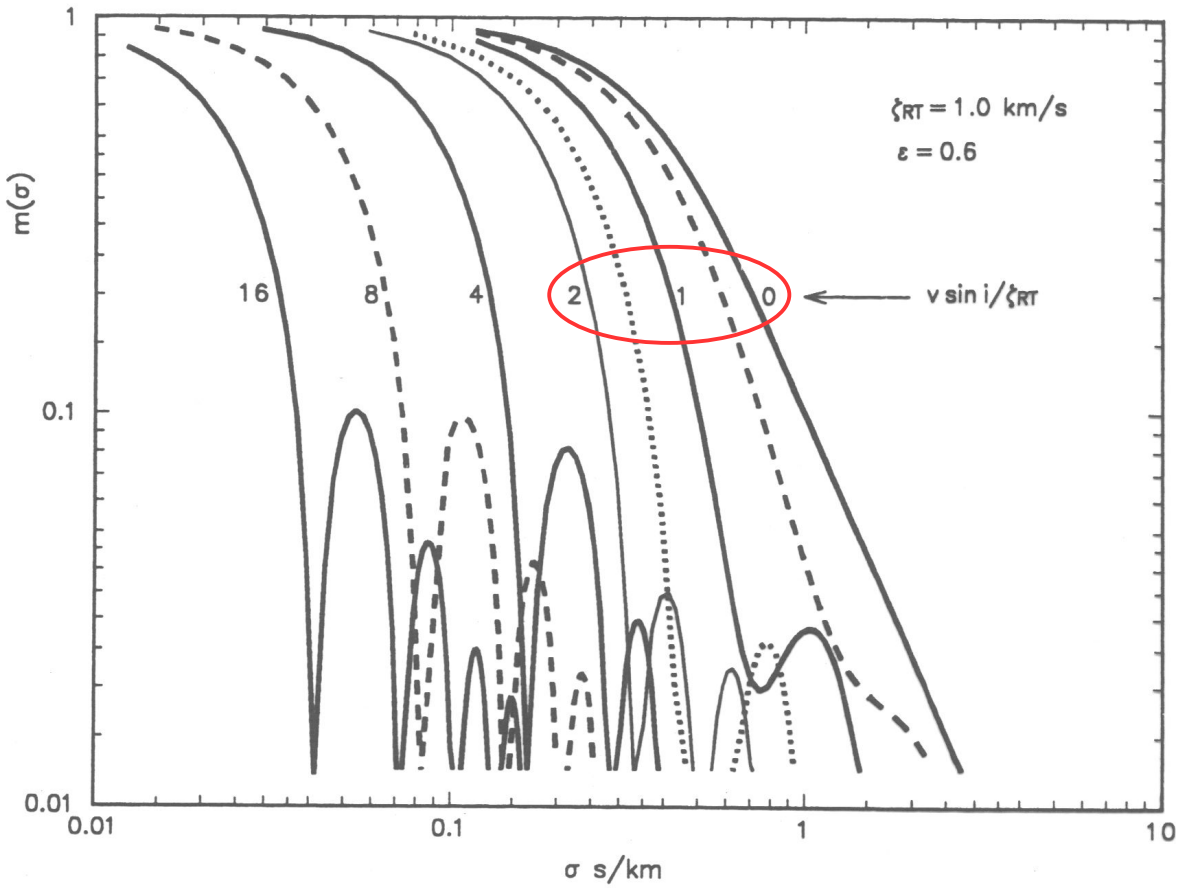

Fig. 18.5. Disk integrations of the combined Doppler shifts of rotation and radial-tangential macroturbulence give the macrobroadening profiles. Their transforms are shown here for several ratios of $v \sin i$ to ζ_{RT}, as labeled.

(from Gray 2005)

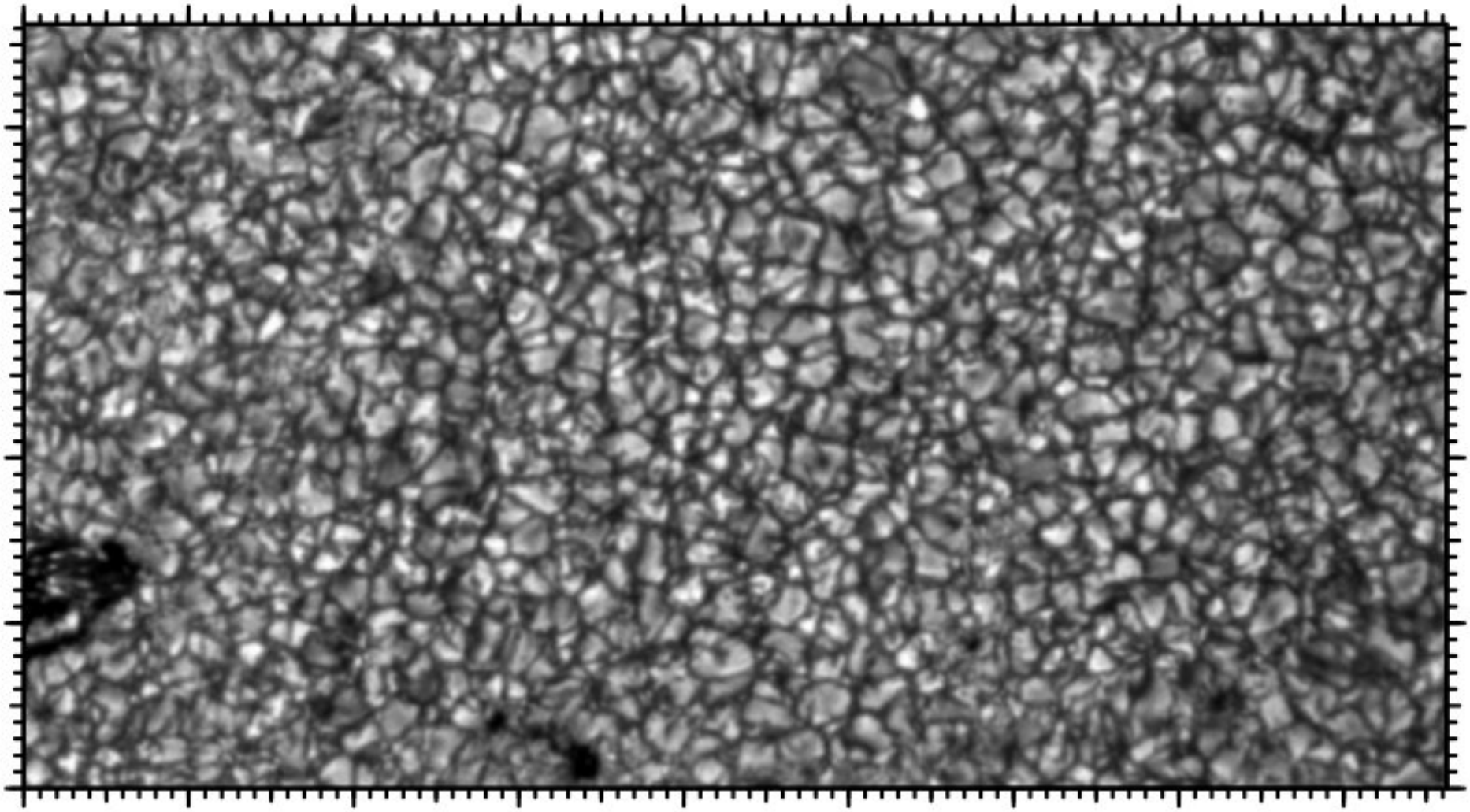

from Rutten and Schrijver (1994)

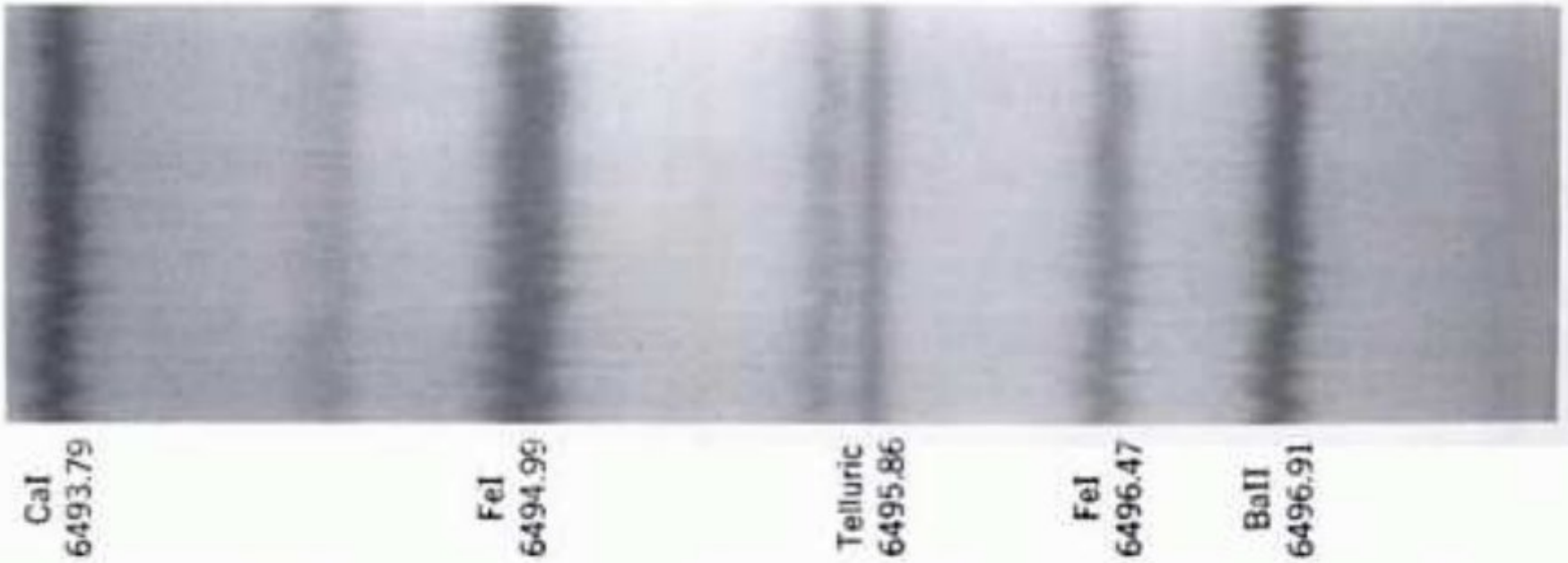

Fig. 17.4. Solar spectra show the individual Doppler shifts of convective cells according to the position of the cells along the entrance slit of the spectrograph. Notice the telluric line that has no wiggles. Photograph courtesy of the McMath-Hulbert Observatory.

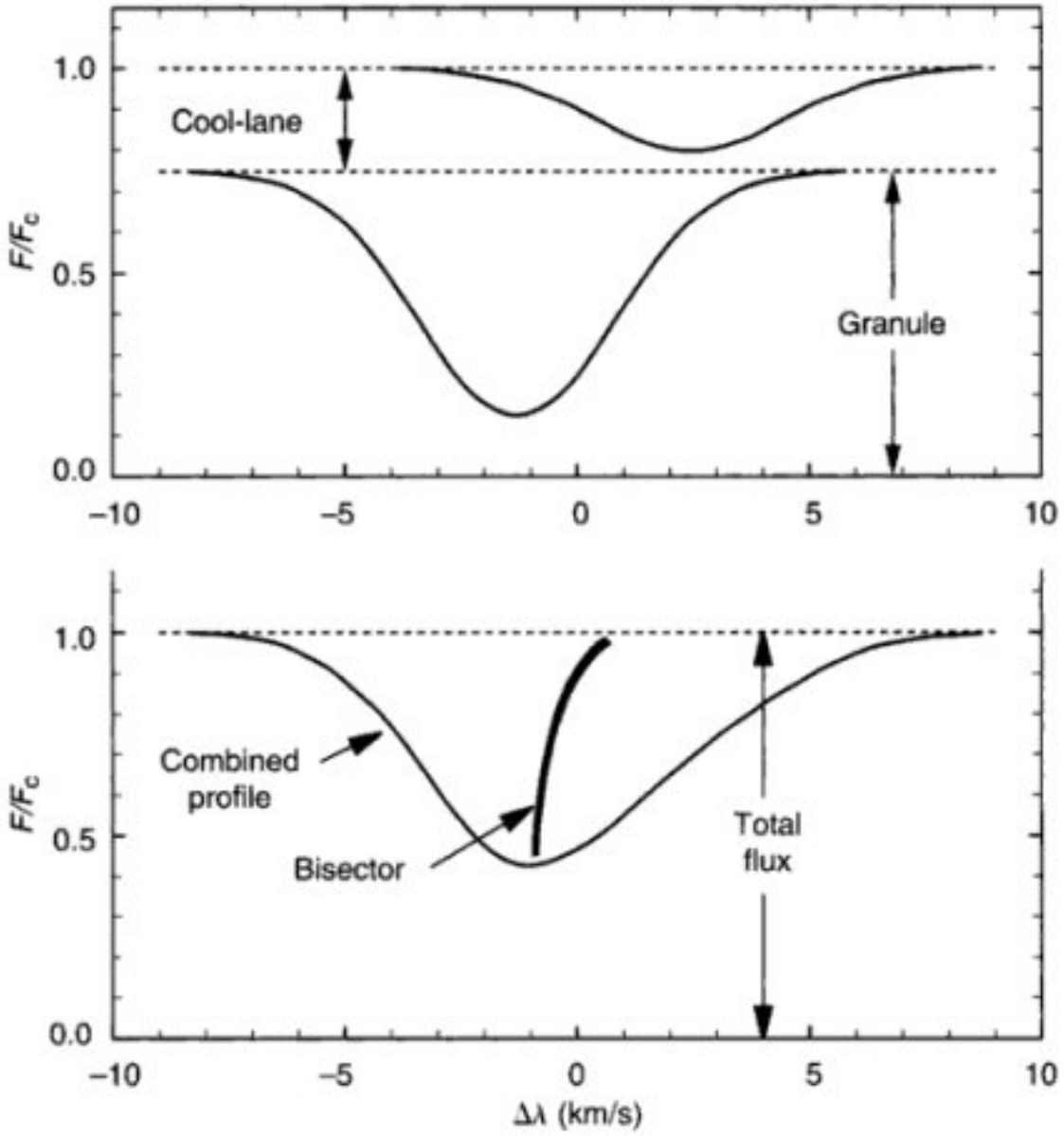

(from Gray 2005)

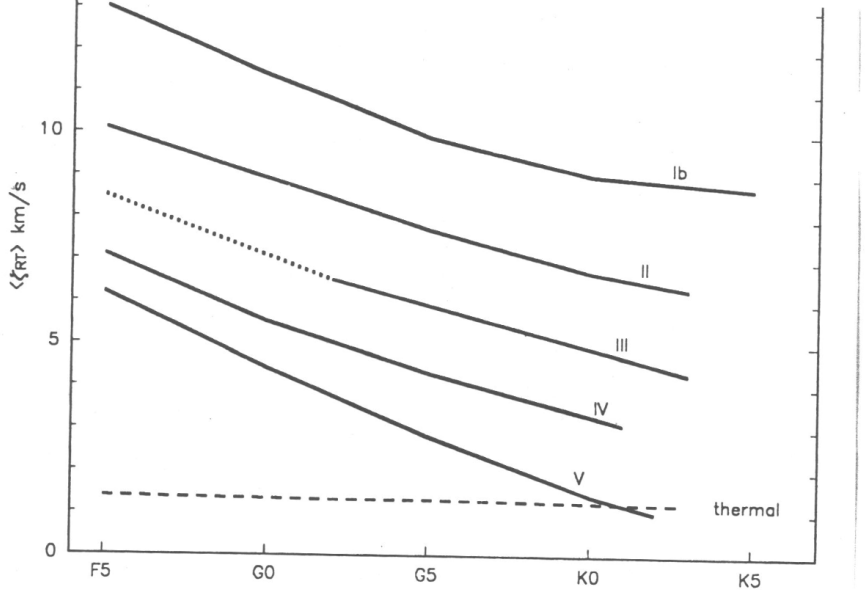

Fig. 18.9. Radial-tangential macroturbulence dispersion increases with effective temperature and with luminosity. Mean values are shown here. Only for cool dwarfs does the macroturbulence become comparable to the thermal broadening.

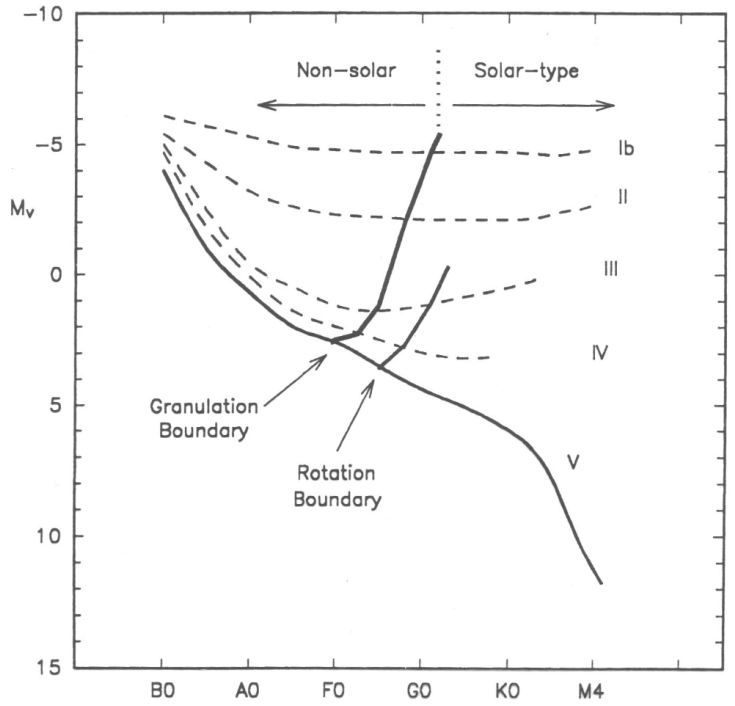

Fig. 18.19. The granulation boundary is the locus of vertical bisectors. The bisectors are of the solar type on the right, but are reversed in slope and curvature on the left. The granulation boundary separates 'hot' stars from 'cool' ones. The rotation boundary from Fig. 17.21 is shown for comparison.

(from Gray 2005)